CHEMICAL ENGINEERING TRANSACTIONS
VOL. 113, 2024
A publication of AIDIC
The Italian Association of Chemical Engineering
Online at www.cetjournal.it
Guest Editors: Jeng Shiun Lim, Bohong Wang, Guo Ren Mong, Petar S. Varbanov

ISBN 979-12-81206-14-4; **ISSN** 2283-9216
DOI: 10.3303/CET24113084

Porous Carbon Synthesis from Oil Palm Waste Pyrolysis for Energy Storage Applications

Pin Shern Wong[a], Jing Jing Jong[a], Guo Ren Mong[a,*], Andrew Kay Lup Ng[a], Nahrul Hayawin Zainal[b], Singh Ramesh[c]

[a]School of Energy and Chemical Engineering, Xiamen University Malaysia, Jalan Sunsuria, Bandar Sunsuria, 43900, Sepang, Selangor, Malaysia
[b]Malaysian Palm Oil Board, 6 Persiaran Institusi, Bandar Baru Bangi, 43000 Kajang, Selangor, Malaysia.
[c]Department of Mechanical Engineering, Faculty of Engineering, University of Malaya, 50603 Kuala Lumpur, Malaysia
guoren.mong@xmu.edu.my

The Palm Oil sector is one of the biggest biomass industries in Malaysia with approximately 140 million tonnes of oil palm waste produced in 2022. A proper and systematic approach is required to manage and valorize this waste if Malaysia intends to fully utilize biomass resources. Pyrolysis procedures have emerged as an exceptionally encouraging method to transform biomass into valuable products. The critical benefit of this technique lies in its proficient capability to thermally decompose biomass at elevated temperatures without the presence of oxygen. This technology facilitates the synthesis of biochar, bio-oil, and syngas, which hold critical value in different applications. This work investigates the potential of valorizing oil palm wastes (OPW) into porous carbon via catalytic pyrolysis. The study intends to discover a green feedstock for energy storage applications through a sustainable technology. OPW will first be treated with Iron(III) nitrate and Cobalt(II) nitrate salts to incorporate the Fe, Co, and FeCo catalyst particles. The pretreated OPW will then undergo pyrolysis in an inert environment at 600 °C. The results showed biochar yields of 36.33 %, 31.47 % and 34.92 % for Fe, Co, and FeCo catalysts, respectively. Electrochemical tests showed that the specific capacitances for Fe-600, Co-600, and FeCo-600 were 66.3746, 64.2444, and 71.2457 F/g, respectively. The Nyquist plots obtained showed that FeCo-600 possessed the lowest contact resistance and highest capacitive properties.

1. Introduction

Being the most traded oil for food and biodiesel production, the supply and demand for palm oil are expected to rise in accordance with the world's population growth (Wahid et al., 2007). It was recorded that the global palm oil consumption increased from 2015 to 2022, with an average increment of 3.68 % per annum (Shahbandeh et al., 2023). However, Nizamuddin et al. (2016) stated that the palm oils generated only account for 10 % of the oil palm trees, and the rest (90 %) are regarded as agricultural waste. In 2022, the Malaysian Palm Oil Board estimated that over 140 million tonnes of oil palm waste (OPW) were generated in Malaysia from agricultural activities, with oil palm trunk (OPT) and fronds (OPF) accounting for 75 % of the wastes (National Biomass Action Plan 2023-2030, 2023). The remaining 25 % comprises other parts such as empty fruit bunches (EFB), palm kernel shells (PKS) and mesocarp fibres (MF) (Hamzah et al., 2019). As such, utilization of the waste generated from palm oil for the synthesis of high-value products is worthy of investigation.

On the positive side, the increasing global emphasis on sustainable development and environmental conservation has intensified interest in the valorization of oil palm waste materials. Ferreria et al. (2020) synthesized biofuels via slow pyrolysis of EFB. The authors revealed that the synthesized bio-oil was rich in hexadecenoic acid, nonane, and phenol. Further analysis illustrated the potential of the bio-oil as biodiesel-based additives. OPF was also valorized to synthesize mesoporous biochar. The authors discovered that the synthesized biochar has excellent phenol removal ability (Lawal et al., 2020). Razali and Kamarulzaman (2020) utilized OPT to synthesize biochar. The synthesized biochar was found to provide a 49.5 % reduction in chemical oxygen demand (COD) in POME wastewaters. Khanday et al. (2016) pyrolyzed oil palm mesocarp fibres and

Paper Received: 25 May 2024; Revised: 6 August 2024; Accepted: 28 October 2024
Please cite this article as: Wong P.S., Jong J.J., Mong G.R., Ng A.K.L., Zainal N.H., Ramesh S., 2024, Porous Carbon Synthesis from Oil Palm Waste Pyrolysis for Energy Storage Applications, Chemical Engineering Transactions, 113, 499-504 DOI:10.3303/CET24113084

reported that the synthesized bio-oil contained low oxygen content, thus highlighting the potential for fuel-grade bio-oil. These studies illustrate the potential of transforming OPWs into valuable bio-products.
In recent years, the transformation of OPW into supercapacitor electrode materials has been gaining popularity. Liu et al. (2019) utilized potassium hydroxide (KOH) for the activation process, and the authors discovered that the highest surface area of 1755 m^2/g was achieved for biochar obtained with 300 °C pre-carbonization. Lee et al. (2023) synthesized activated carbon from the orange peel with phosphoric acid as the catalyst, and the derived biochar possessed the highest specific capacitance of 57.7056 F/g at a 50 mV/s scan rate.
This work focuses on the synthesis of supercapacitor electrode materials using PKS activated with iron (Fe) and cobalt (Co) catalysts via pyrolysis. Limited studies have been conducted to investigate the effects of the mixture of Fe and Co catalysts in activating the biomass, which is poised to augment the electrochemical properties of the generated char. In this work, a comparison between Fe, Co, and Fe-Co-treated PKS to evaluate the specific capacitances and energy densities of the fabricated electrodes was conducted. Electrochemical impedance spectroscopy (EIS) to obtain Nyquist plots was utilized to evaluate the capacitive and resistive properties of the synthesized electrodes.

2. Methodology

2.1 Materials

Palm kernel shells (PKS) were collected from Stesen Penyelidikan MPOB/UKM. Cobalt nitrate hexahydrate, $Co(NO_3)_2{\cdot}6H_2O$ (R&M Chemicals), iron nitrate nonahydrate, $Fe(NO_3)_3{\cdot}9H_2O$ (R&M Chemicals), potassium hydroxide, KOH (R&M Chemicals), carboxymethyl cellulose, CMC (R&M Chemicals) and conductive carbon were used without further modification. Nitrogen gas (99.9 % N_2, Alpha Gas) was utilized to ensure an inert atmosphere for pyrolysis.

2.2 Preparation of feedstock

Dried PKS were pulverized and sieved with a 100-micron sieve. 1 M of cobalt nitrate solution, $Co(NO_3)_2{\cdot}6H_2O$, was prepared by dissolving cobalt nitrate in 100 mL of deionized (DI) water. 25 g of PKS powder was then immersed in the cobalt nitrate solution, and the solution was stirred constantly at 80 °C for 3 h. The mixture was then dried in oven at 100 °C for 12 h. The same method was used to prepare two additional feedstocks: one with a 1 M iron nitrate solution, $Fe(NO_3)_3{\cdot}9H_2O$, as the catalyst, and the other with a hybrid catalyst solution consisting of $Co(NO_3)_2{\cdot}6H_2O$ and $Fe(NO_3)_3{\cdot}9H_2O$ at a 1:1 molar ratio.

2.3 Catalytic pyrolysis of pretreated PKS

45 g of the treated PKS was transfer to a ceramic boat and inserted into a tube furnace (Thermolyne F21100 Tube Furnace). The setup was purged for 10 min using N_2 gas at 2 L/min. The pyrolysis experiment was conducted at 600 °C with a ramping rate of 10 °C/min. During pyrolysis, the N_2 gas flow was fixed at 1 L/min and the residence time for the feedstock was 1 h. After pyrolysis, the setup was allowed to cool naturally under continuous gas flow. Biochar was removed manually from the ceramic boat and its yield was calculated based on Eq(1).

$$Yield\ (\%) = \frac{Mass\ of\ biochar\ (g)}{Mass\ of\ pretreated\ PKS\ (g)} \times 100 \quad (1)$$

2.4 Post-treatment and characterization of bio char

3 M hydrochloric acid (HCl) was prepared by adding 24.6 mL of concentrated HCl to 100 mL of DI water, and the biochar was added to the dilute HCl at a ratio of 5 g biochar to 100 mL 3 M HCl. The biochar was immersed in the HCl solution for 2 h and sonicated for 30 min at room temperature. The sonicated char was then rinsed with DI water until a pH of 7 was obtained. The char was then vacuum filtered and dried overnight in oven at 100 °C. The biochar obtained were denoted as Fe-600, Co-600, and FeCo-600 based on the catalyst applied for pretreatment. Scanning electron microscope (SEM) and Fourier-transform infrared (FTIR) spectroscopy were also utilized to evaluate the morphology and characteristics of the biochar.

2.5 Two-electrode coin cell fabrication

PKS char, conductive carbon, and CMC powder were mixed in a pestle and mortar at a ratio of 8:1:1. DI water was applied as the solvent. The carbon slurry was prepared by grinding the PKS char powder and conductive carbon, then added with the CMC binder powder and DI water. The slurry was mixed until no large particles were observed and coated onto a current collector, which in this experiment was copper foil. A doctor blade was utilized at a coating thickness of 30 µm to ensure even coating thickness. The carbon slurry was dried at 50 °C

and punched into circles with 12-mm diameters with a hydraulic press. The coin cell was assembled in accordance with the following components: negative terminal cell casing, anode, separator, cathode, spacer, spring, and positive terminal cell casing. 6 M KOH solution was used as the aqueous electrolyte in this experiment.

2.6 Electrochemical measurement

Electrochemical measurements for the two-electrode coin cell were analyzed using a potentiostat (Ametek VersaSTAT 4 Potentiostat Galvanostat) with a coin cell holder. The working and sense electrodes were connected to the positive terminal of the cell holder, and the counter and reference electrodes were connected to the negative terminal. The ground electrode was not utilized for this test. Cyclic voltammetry (CV) tests and EIS tests were performed to evaluate the chemical performance of the assembled coin cells. The CV tests were conducted in a potential window of 1 V at different scan rates, and the EIS tests were conducted from 100,000 Hz to 0.01 Hz. The specific capacitance and the energy density were evaluated using Eq(2) and Eq(3) (Zhang et al., 2014).

$$C_s = \frac{2\int_{V_a}^{V_b} I dV}{mv(V_b - V_a)} \tag{2}$$

where C_s is the specific capacitance (F/g); V_a and V_b are the low and high potential limit (V); I is the discharge current; m is the mass of the active materials for both electrodes (g); and v is the scan rate (V/s).

$$E = \frac{1}{8} C_s \Delta V^2 \tag{3}$$

where E is the energy density (Wh/kg) and $\Delta V$is the potential window (V).

3. Results and discussion

3.1 Surface morphology of the pyrolyzed carbon

Figure 1 illustrates the surface morphology of Fe-600, Co-600, and FeCo-600 chars, all of which exhibit pore formation (circled in red). However, the pores are inconsistent and not uniformly distributed across the samples, likely due to variations in the catalyst to biomass ratio used during the experiment. Tu et al. (2023) investigated this effect and found that a moderate catalyst to biomass mass ratio (2:1 to 4:1) facilitates the formation of meso- and micropores. However, a low catalyst to biomass ratio results in minimal pore formation, indicating incomplete or ineffective chemical activation. Since a low catalyst to biomass ratio (1 M catalyst solution impregnation) was used in this study, it is possible that the used ratio was not optimal in synthesizing biochar with evenly distributed porous surfaces. These findings suggest that the catalyst to biomass ratios could be further optimized to achieve more consistent and uniform pore structures in the pyrolyzed char.

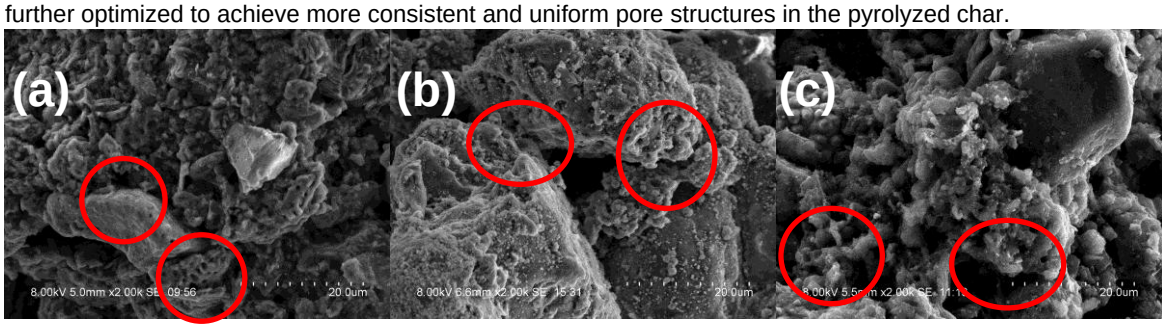

Figure 1: Surface morphology of (a) Fe-600; (b) Co-600; and (c) FeCo-600

3.2 Fourier-transform infrared (FTIR) spectroscopy

The FTIR spectra for Fe-600, Co-600 and FeCo-600 are shown in Figure 2. The peaks illustrated in the range of 3900 to 3800 cm^{-1} indicated that free hydroxyl (-OH) was detected. This could be attributed to the presence of water vapors in the instrument or the sample (Aroke et al., 2013). The peaks from 3700 to 3500 cm^{-1} showed that OH group stretching was detected. No obvious functional groups were detected between 3500 and 2000 cm^{-1}. However, multiple peaks were detected from 1800 to 1400 cm^{-1}, revealing that the vibration of C=C bonds was present and that aromatic compounds and alkanes were detected. The transmittance peaks observed from 1350 to 1000 cm^{-1} indicate that C-O bond stretching was detected (Baby et al., 2019). These vibrations could be attributed to the presence of ethers, alcohol, anhydrides, and esters (Mohamed et al., 2017). The peaks between bands 950 and 620 cm-1 can be attributed to the stretches resulting from C-C bonds (Baby et al.,

2021). When compared to raw PKS, Ikubanni et al., (2020) stated that functional groups such as C-H, C=O, and C-O vanished when the biomass underwent high temperatures. The authors attributed this to the decomposition of structural components in the palm kernel shell, such as lignin, hemicellulose, and cellulose.

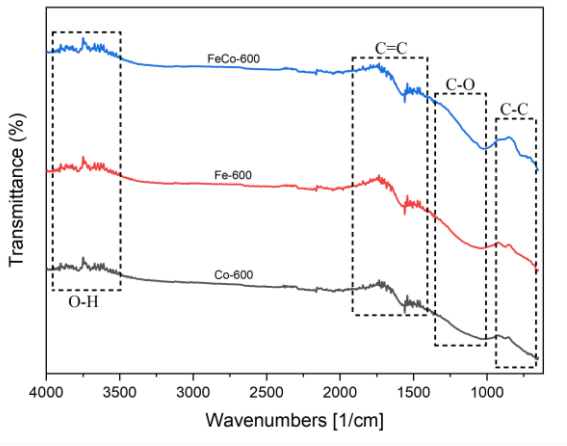

Figure 2: FTIR spectra of PKS biochar

3.3 Cyclic voltammetry tests

Figure 3 shows the CV curves for the samples at a constant voltage window of 1 V, and different scan rates ranging from 10 mV/s to 200 mV/s. It was observed that FeCo-600 possessed the largest CV curve as shown in the comparison plot in Figure 3a, indicating that the sample showed the highest capacitance. However, the CV curves for Fe-600 (Figure 3b), Co-600 (Figure 3c), and FeCo-600 (Figure 3d) were not pseudo-rectangle shaped, indicating that the transfer kinetics have deviations from the ideal case. Also, the distortions in the CV curves increased as the scan rates were elevated. This could be attributed to the fact that the ion transfer kinetics were limited by insufficient pores in the char (Ma et al., 2021). Azman et al. (2018) also stated that the deviations from pseudo-rectangular shapes could be caused by Faradaic reactions, which the reactions involve the transfer of electrons between an electrode and a chemical species in an electrochemical cell, resulting in a redox process. Chen (2013) mentioned that such reactions could be induced by the presence of transition metal oxides. Table 1 shows the integrated areas of the CV curves for Fe-600, Co-600, and FeCo-600 at 25 mV/s scan rate. The calculated specific capacitances and energy densities are also tabulated to compare the performances of the synthesized electrodes.The performances and impedance characteristics of the fabricated chars can be evaluated through EIS. Figure 4 shows the EIS plots for Fe-600, Co-600, and FeCo-600. The imaginary component (Zim) represents the capacitive properties of the sample, while the real impedance component (Zre) represents the resistive properties. The semicircle in the Nyquist plots shown in Figure 4b illustrates the charge transfer resistance and double layer capacitance properties of the samples. Fe-600 showed the largest semicircle compared to Co-600 and FeCo-600, indicating that the sample showed the highest resistive behavior and poorest charge transfer properties (Tu et al., 2023). The gradients of the Warburg region (steep part) for the samples, as illustrated in Figure 4a, also provided valuable information. FeCo-600 showed a curve closest to the vertical y-axis, indicating that the sample showed the greatest electrical conductivity and the lowest electrical contact resistance (Yu et al., 2019). Zhang and Shi (2011) also mentioned that supercapacitors behave more like ideal capacitors as the steepness of the curve increases. These findings were supported by the CV curve results, showing FeCo-600 having the highest specific capacitance and energy density. It is envisaged that the electrochemical performance can be augmented by increasing the pyrolysis temperature. Armynah et al. (2019) stated that elevated activation temperatures can lead to increased micropore formation that can improve electrochemical performances.

Table 1: Specific Capacitance and Energy Density for Electrochemical Performance at 25 mV/s Scan Rate

Sample	Integrated Area	Mass (mg)	Specific Capacitance (F/g)	Energy Density (Wh/kg)
Fe-600	0.005227	6.3	66.3746	8.2968
Co-600	0.005782	7.2	64.2444	8.0306
FeCo-600	0.006234	7.0	71.2457	8.9057

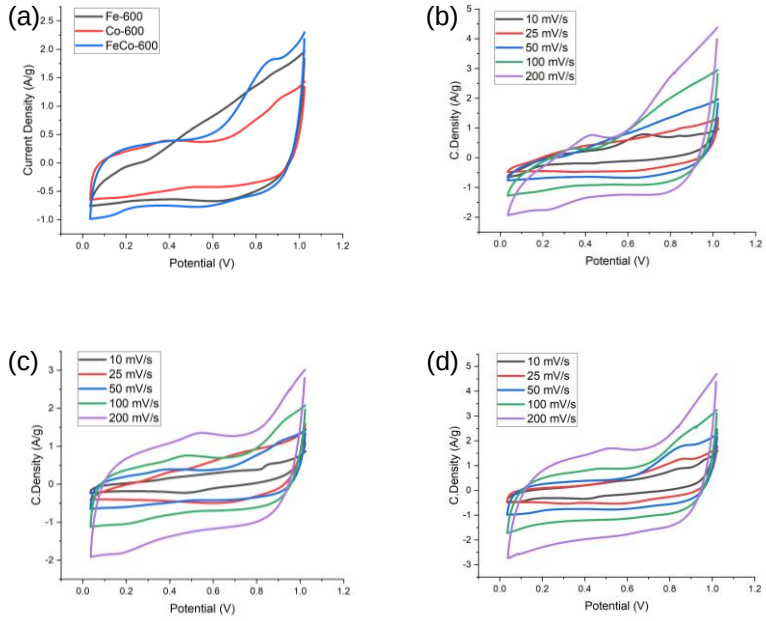

Figure 3: CV tests using symmetrical cells. (a) CV curves of char at 50 mV/s; (b) CV curves of Fe-600 at10 to 200 mV/s; (c) CV curves of Co-600 at10 to 200 mV/s; (d) CV curves of FeCo-600 at 10 to 200 mV/s

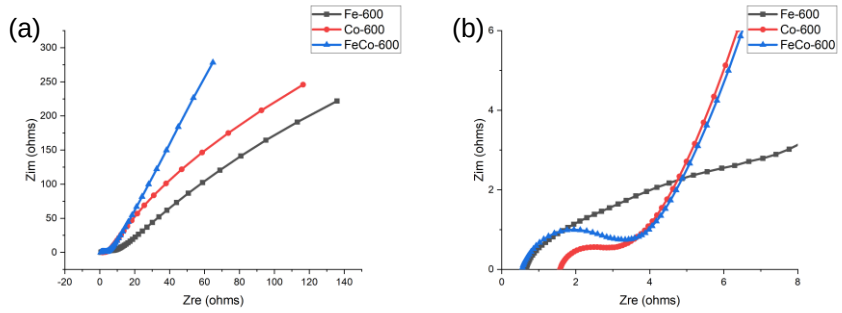

Figure 4: EIS performance of symmetrical cells. (a) Nyquist plot; (b) Enlarged view of Nyquist plot

4. Conclusions

Electrode materials for symmetrical cell supercapacitors were synthesized with Co, Fe, and Fe-Co catalyst activation at 600 °C. The surface morphology of the pyrolyzed char was examined and the FTIR spectra revealed that the chars predominantly possessed C=C containing compounds such as aliphatics and aromatics. The spectra showed that a change in catalyst did not significantly affect the presence of certain functional groups in the char. Cyclic voltammetry tests revealed that Fe-600, Co-600, and FeCo600 illustrated remarkable specific capacitances of 66.37, 64.24, and 71.25 F/g at 25 mV/s scan rate, respectively. The deviation of the CV curves from the ideal shape can be attributed to the presence of faradaic currents induced by the presence of transition metals. Electrochemical impedance spectroscopy tests also revealed that FeCo-600 showed low resistance and great capacitive behaviours. The results showed that FeCo-600 illustrated the best performance for energy storage applications. These findings revealed the potential to valorise OPW as a carbon source and utilize iron and cobalt salts as catalysts for the synthesis of supercapacitor electrode materials.

Acknowledgments

This research was supported by Xiamen University Malaysia through the Xiamen University Malaysia Research Fund [XMUMRF/2022-C9/IENG/0045] and The Malaysia Palm Oil Board [02/B/PKP/139(1449)].

References

Armynah B., Taer E., Djafar Z., Piarah W.H., Tahir D., 2019, Effect of temperature on physical and electrochemical properties of the monolithic carbon-based bamboo leaf to enhanced surface area and specific capacitance of the supercapacitor, International Journal of Electrochemical Science, 14(8), 7076-7087.

Aroke U., Abdulkarim A., Ogubunka R., 2013, Fourier-transform infrared characterization of kaolin, granite, bentonite and barite, ATBU journal of environmental technology, 6(1), 42-53.

Azman N.H.N., Mamat@ Mat Nazir M.S., Ngee L.H., Sulaiman Y., 2018, Graphene‐based ternary composites for supercapacitors, International Journal of Energy Research, 42(6), 2104-2116.

Baby R., Hussein M.Z., Zainal Z., Abdullah A.H., 2021, Functionalized activated carbon derived from palm kernel shells for the treatment of simulated heavy metal-contaminated water, Nanomaterials, 11(11), 313.

Baby R., Saifullah B., Hussein M.Z., 2019, Palm Kernel Shell as an effective adsorbent for the treatment of heavy metal contaminated water, Scientific Reports, 9(1), 18955.

Chen G.Z., 2013, Understanding supercapacitors based on nano-hybrid materials with interfacial conjugation, Progress in Natural Science: Materials International, 23(3), 245-255.

Ferreira M., Oliveira B., Pinheiro W., Correa N., França L., Ribeiro N., 2020, Generation of biofuels by slow pyrolysis of palm empty fruit bunches: Optimization of process variables and characterization of physical-chemical products, Biomass and Bioenergy, 140, 105707.

Hamzah N., Tokimatsu K., Yoshikawa K., 2019, Solid fuel from oil palm biomass residues and municipal solid waste by hydrothermal treatment for electrical power generation in Malaysia: A review, Sustainability, 11(4), 1060.

Ikubanni P., Oki M., Adeleke A., Adediran A., Adesina O., 2020, Influence of temperature on the chemical compositions and microstructural changes of ash formed from palm kernel shell, Results in Engineering, 8, 100173.

Khanday W.A., Kabir G., Hameed B., 2016, Catalytic pyrolysis of oil palm mesocarp fibre on a zeolite derived from low-cost oil palm ash, Energy Conversion and Management, 127, 265-272.

Lee Y.K., Liew C.P., Kiew P.L., Foo B.C.Y., Yeoh W.M., Ho M.Y., 2023, Orange Peel-Derived Activated Carbon as a Potential Electrode Material for Supercapacitor Application, Chemical Engineering Transactions, 106, 1285-1290.

Liu C., Chen W., Li M., Hong S., Li W., Pan M., Wu Q., Mei C., 2019, Rapid microwave activation of waste palm into hierarchical porous carbons for supercapacitors using biochars from different carbonization temperatures as catalysts, RSC advances, 9(34), 19441-19449.

Ma Z.W., Liu H.Q., Lü Q.F., 2021, Porous biochar derived from tea saponin for supercapacitor electrode: Effect of preparation technique, Journal of Energy Storage, 40, 102773.

Mohamed M.A., Jaafar J., Ismail A., Othman M., Rahman M., 2017, Fourier transform infrared (FTIR) spectroscopy, In Membrane characterization (pp. 3-29). Elsevier.

National Biomass Action Plan 2023-2030, 2023, Ministry of Plantation and Commodities (KPK), Putrajaya, Malaysia.

Nizamuddin S., Shrestha S., Athar S., Ali B.S., Siddiqui M.A., 2016, A critical analysis on palm kernel shell from oil palm industry as a feedstock for solid char production, Reviews in Chemical Engineering, 32(5), 489-505.

Razali N., Kamarulzaman N.Z., 2020, Chemical characterizations of biochar from palm oil trunk for palm oil mill effluent (POME) treatment, Materials Today: Proceedings, 31, 191-197.

Shahbandeh M., 2023, Palm oil usage worldwide 2015/16-2022/23, Statista <statista.com/statistics/274127/world-palm-oil-usage-istribution/#statisticContainer> accessed 28.05.2024.

Tu J., Qiao Z., Wang Y., Li G., Zhang X., Li G., Ruan D., 2023, Biomass-based porous carbon for high-performance supercapacitor electrode materials prepared from Canada goldenrod, Journal of Energy Storage, 73, 109268.

Wahid M.B., Lim W., Mohd Arif S., 2007, Technological development and new growth areas of the oil palm industry, Oil Palm Industry Economic Journal, 7(1), 1-8.

Yu J., Fu N., Zhao J., Liu R., Li F., Du Y., Yang Z., 2019, High specific capacitance electrode material for supercapacitors based on resin-derived nitrogen-doped porous carbons, ACS omega, 4(14), 15904-15911.

Zhang L., Shi G., 2011, Preparation of highly conductive graphene hydrogels for fabricating supercapacitors with high rate capability, The Journal of Physical Chemistry C, 115(34), 17206-17212.

Zhang Z.J., Xie D.H., Cui P., Chen X.Y., 2014, Conversion of a zinc salicylate complex into porous carbons through a template carbonization process as a superior electrode material for supercapacitors. RSC advances, 4(13), 6664-6671.